New Journal of Physics
The open access journal at the forefront of physics

Deutsche Physikalische Gesellschaft DPG IOP Institute of Physics

PAPER • OPEN ACCESS

Ghost imaging with engineered quantum states by Hong–Ou–Mandel interference

To cite this article: Nicholas Bornman *et al* 2019 *New J. Phys.* **21** 073044

IOP Publishing New J. Phys. 21 (2019) 073044 https://doi.org/10.1088/1367-2630/ab2f4d

New Journal of Physics
The open access journal at the forefront of physics

Deutsche Physikalische Gesellschaft DPG
IOP Institute of Physics

Published in partnership with: Deutsche Physikalische Gesellschaft and the Institute of Physics

OPEN ACCESS

RECEIVED
1 April 2019

REVISED
19 June 2019

ACCEPTED FOR PUBLICATION
3 July 2019

PUBLISHED
23 July 2019

PAPER

Ghost imaging with engineered quantum states by Hong–Ou–Mandel interference

Nicholas Bornman[1], **Shashi Prabhakar**[1,2], **Adam Vallés**[1,3,4], **Jonathan Leach**[5] and **Andrew Forbes**[1]

[1] School of Physics, University of the Witwatersrand, Private Bag 3, Wits 2050, South Africa
[2] CSIR National Laser Centre, PO Box 395, Pretoria 0001, South Africa
[3] Graduate School of Advanced Integration Science, Chiba University, 1-33 Yayoi-cho, Inage-ku, Chiba 263-8522, Japan
[4] Molecular Chirality Research Center, Chiba University, 1-33, Yayoi-cho, Inage-ku, Chiba 263-8522, Japan
[5] IPaQS, SUPA, Heriot-Watt University, Edinburgh EH14 4AS, United Kingdom

E-mail: adam.vallesmari@wits.ac.za

Keywords: ghost imaging, Hong-Ou-Mandel interference, quantum optics, state symmetry

Supplementary material for this article is available online

Abstract

Traditional ghost imaging experiments exploit position correlations between correlated states of light. These correlations occur directly in spontaneous parametric down-conversion, and in such a scenario, the two-photon state usually used for ghost imaging is symmetric. Here we perform ghost imaging using an anti-symmetric state, engineering the two-photon state symmetry by means of Hong–Ou–Mandel interference. We use both symmetric and anti-symmetric states and show that the ghost imaging setup configuration results in object-image rotations depending on the state selected. Further, the object and imaging arms employ spatial light modulators for the all-digital control of the projections, being able to dynamically change the measuring technique and the spatial properties of the states under study. Finally, we provide a detailed theory that explains the reported observations.

1. Introduction

Ghost imaging was first performed by Pittman *et al* [1], in which entanglement was utilized as the source of spatial correlations between a pair of separate photons. In quantum ghost imaging, one photon of the pair interacts with an arbitrary object and is collected with a bucket detector with no spatial resolution. The other photon, in the imaging arm, does not interact with the object but rather is sent directly to a spatially-resolving device for detection, usually a 2D scanning detection system or a camera. Despite neither photon being able the recover the shape of the object by itself, an image can be reconstructed when measuring in coincidences due to the spatial correlations created prior to the interaction with the object, i.e. within the nonlinear crystal.

The first ghost imaging tests made use of entanglement as the source of spatial correlations, such as those arising from the spontaneous parametric down-conversion (SPDC) process [2]. However, classical intensity correlations from a thermal light source have also been used to demonstrate ghost imaging [3–5], showing the analogy between the two scenarios [6, 7]. Subsequently, ghost imaging has been studied from a computational perspective (a technique which only requires bucket detectors) [8, 9] and using compressive sensing to reduce the number of required measurements [10]. Ghost imaging has also been observed in various degrees of freedom (DoF), such as the orbital angular momentum (OAM) of light [11], correlations in the time domain [12], in momentum-position [13] and spectral DoF [14]. 3D ghost images have been reconstructed using single pixel detectors [15], and ghost imaging has even been studied in the presence of turbulence [16]. See [17, 18] for comprehensive reviews. Recently, the concept of ghost imaging was extended to entanglement swapped photons, demonstrating ghost imaging with initially independent photons [19]. In this case the role of state symmetry was crucial to the outcome of the object/image contrast.

Here we demonstrate a new form of ghost imaging where the object and image arms are placed after a Hong–Ou–Mandel (HOM) interference filter [20], allowing the biphoton imaging to be carried out using either

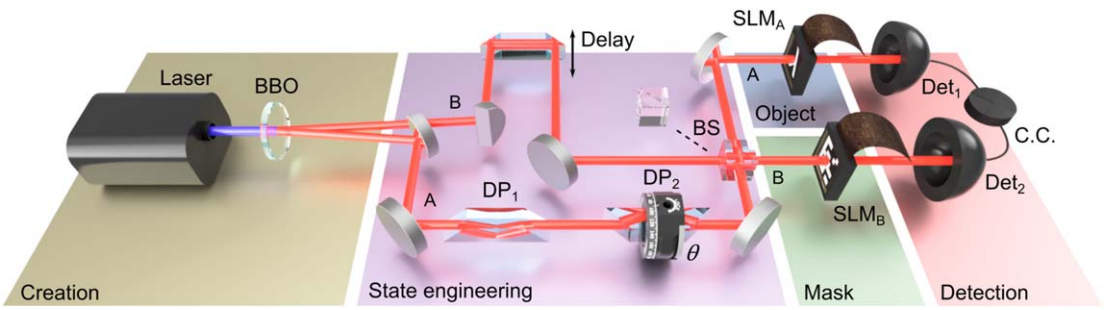

Figure 1. Detailed experimental setup description, comprising the creation (golden), state engineering (purple), object (blue), mask (green) and detection (red) steps. BBO: nonlinear crystal; $DP_{1\text{ and }2}$: dove prisms; BS: 50:50 beamsplitter; $SLM_{A\text{ and }B}$: spatial light modulators; $Det_{1\text{ and }2}$: bucket detectors formed by interference filters, few-mode fibres and avalanche photo-diodes; C.C.: coincidence counter.

symmetric or anti-symmetric states. Furthermore, we employ spatial light modulators (SLMs) to dynamically control both the object and image, in particular, using digitally-controlled holograms on the image arm to reconstruct the object without a mechanical scanning system or a spatially-resolved camera. We show that our ghost imaging setup including the HOM filter results in the reconstruction of an image comprised of a 'double object', with each reconstructed object rotated in opposite directions. This is explained by the action of the symmetry selection step comprising a beamsplitter (BS) and Dove prisms.

2. Experiment

We start describing the experimental setup in figure 1 to easily identify the role of each optical element involved later on in the Theory section. The experiment is divided conceptually into three sections. In the first, an entangled biphoton state is produced using a SPDC photon pair source, resulting in a state that is always symmetric. In the second, we pass the photon pair through a quantum state engineering system comprising Dove prisms (to control state phases θ) and a HOM interference filter to single out specific states based on their symmetry. Finally, in the third part we perform ghost imaging using the engineered two-photon state, consisting of the object and mask projections and photon pair detection. A detailed description of the experimental setup is given in the supplementary material, available online at stacks.iop.org/NJP/21/073044/mmedia.

We employ tools common in computational ghost imaging, namely digital projections for the image reconstruction, allowing the use of two bucket detectors and removing the need for cameras or mechanical scanning systems. To perform the ghost imaging measurements, the binary object, O, that we wish to reconstruct is encoded on SLM_A, and the scan is performed by dynamically modifying the hologram encoded on SLM_B. The different procedures used to reconstruct the image, single pixel and random mask scans, are introduced in the Results section.

3. Theory

Spatially-entangled photon pairs are generated in the nonlinear crystal (BBO). After propagating along the optical elements comprising the symmetry filter, the photons of each pair, A and B, are sent to the SLM screens. SLM_A is masked with a binary object O of our choosing, and SLM_B is used to perform measurements. Based on said measurements on photon B, O can be reconstructed when detected in coincidence with photon A.

To study the effect of state symmetry on the reconstructed object, we first study the setup using the OAM basis of the photons [21]. Any set of spatial modes which form a basis can be used to express a mode of light with an arbitrary spatial profile, e.g. the Laguerre–Gaussian, or Hermite-Gaussian modes. It is also evident that any arbitrary state can be written as the sum of a symmetric part and an anti-symmetric part. The effect that a state symmetry has on, for example, coincidence events in an entanglement experiment has recently been studied [22], where it was shown how to control the spatial state symmetry by exploiting an HOM interferometric measurement [20], also known as an HOM filter. Such techniques work regardless of the spatial basis [23]. The HOM filter passes only anti-symmetric states when conditioned on coincidences and the symmetry of the input state is tuned by adjusting the relative phases using two Dove prisms rotated by an angle of θ relative to one another.

To begin, consider the state generated by SPDC at the crystal plane in the OAM basis

$$|\Psi\rangle = \sum_{\ell} a_{\ell} |\Psi_{\ell}^{+}\rangle, \tag{1}$$

with $|\Psi_{\ell}^{+}\rangle = \frac{1}{\sqrt{2}}\{|\ell\rangle_A|-\ell\rangle_B + |-\ell\rangle_A|\ell\rangle_B\}$, and a_{ℓ} the appropriate amplitude. The presence of the Dove prisms at a relative angle θ in path A has the effect $|\ell\rangle_A \rightarrow |\ell\rangle_A e^{i2\ell\theta}$, in which case equation (1) transforms to

$$\begin{aligned} |\Psi\rangle &\rightarrow \sum_{\ell} \frac{a_{\ell}}{\sqrt{2}}(|\ell\rangle_A|-\ell\rangle_B e^{i2\ell\theta} + |-\ell\rangle_A|\ell\rangle_B e^{-i2\ell\theta}) \\ &= \sum_{\ell} a_{\ell}(|\Psi_{\ell}^{+}\rangle \cos(2\ell\theta) + i|\Psi_{\ell}^{-}\rangle \sin(2\ell\theta)). \end{aligned} \tag{2}$$

When the relative angle is set to $\theta = \frac{\pi}{4}$, the only $|\Psi_{\ell}^{+}\rangle$ ($|\Psi_{\ell}^{-}\rangle$) terms that survive are those with ℓ even (odd). With this state passed through the HOM filter, only the anti-symmetric modes (i.e. $|\Psi_{\ell}^{-}\rangle$, those with odd ℓ values) remain when conditioned on coincidences after the filter [22]. All symmetric states are removed, since they result in no coincidences.

One might ask whether such symmetry filtering holds when any DoF other than OAM is considered. Symmetry is an intrinsic property of a quantum state: a state which is (anti-)symmetric in one basis is (anti-) symmetric in all bases (see supplementary material). Hence, we can express a state in any basis we choose without affecting the symmetry. When considering quantum imaging of arbitrary images, in which information is encoded in the transverse position of every pixel the image is comprised, these pixels are most easily described using a transverse position vector. Hence, it is intuitive to describe imaging in the *position basis*. With this in mind, equation (1) can be re-expressed as

$$|\Psi\rangle = \sum_{\boldsymbol{r}\in\mathcal{S}} c(\boldsymbol{r})|\boldsymbol{r}\rangle_A|\boldsymbol{r}\rangle_B, \tag{3}$$

where the sum runs over all SLM pixels, a set we call $\mathcal{S}$. We consider this discrete case since the SLM itself consists of discrete pixels. Here $c(\boldsymbol{r})$ is the probability amplitude for photons A and B to be found in the crystal plane at the transverse position $\boldsymbol{r} = (x, y)$; they have the same position since they originate at the same point in the crystal.

Photon A passes through two Dove prisms (which are initially set to have a relative angle of $\theta = 0$). Later, when one of the Dove prisms in path A is rotated at an angle θ with respect to the other, $R(2\theta)$ will represent a rotation of the transverse position of photon A (for a setup without the Dove prisms, or with $\theta = 0$, we have $R(2\theta) = \mathbb{I}$). The explicit θ dependence of R is suppressed for brevity. Note also that we assume paths A and B have the same path length unless stated otherwise. Therefore at the BS plane equation (3) becomes

$$|\Psi\rangle \rightarrow \sum_{\boldsymbol{r}} c(\boldsymbol{r})|R\boldsymbol{r}\rangle_A|\boldsymbol{r}\rangle_B. \tag{4}$$

In the absence of a BS and hence an HOM filter, the SLM is placed at the crystal plane and so our 'no BS' state, $|\Psi_{\mathrm{nbs}}\rangle$, at the SLM plane is

$$|\Psi_{\mathrm{nbs}}\rangle = \sum_{\boldsymbol{r}} c(\boldsymbol{r})|R\boldsymbol{r}\rangle_A|\boldsymbol{r}\rangle_B, \tag{5}$$

which shows a rotation of the transverse position of photons in path A. In such a case, it is predicted that the outcome will match that of a conventional ghost imaging experiment, save for the measured image being rotated by an angle of 2θ relative to the object. This is a corollary of the main study.

3.1. Ghost imaging with an HOM filter

In the presence of a 50:50 BS for HOM interference, and accounting for the number of mirror reflections in each path, the action of the filter is

$$|\boldsymbol{r}\rangle_A \rightarrow \frac{1}{\sqrt{2}}[|\boldsymbol{r}\rangle_A + |\boldsymbol{r}\rangle_B]; \;\; |\boldsymbol{r}\rangle_B \rightarrow \frac{1}{\sqrt{2}}[|\boldsymbol{r}\rangle_B - |\boldsymbol{r}\rangle_A], \tag{6}$$

so that our 'BS' state, $|\Psi_{\mathrm{bs}}\rangle$, is

$$\begin{aligned} |\Psi_{\mathrm{bs}}\rangle &= \frac{1}{2}\sum_{\boldsymbol{r}} c(\boldsymbol{r})[|R\boldsymbol{r}\rangle_A + |R\boldsymbol{r}\rangle_B][|\boldsymbol{r}\rangle_B - |\boldsymbol{r}\rangle_A] \\ &= \frac{1}{2}\sum_{\boldsymbol{r}} c(\boldsymbol{r})[|R\boldsymbol{r}\rangle_A|\boldsymbol{r}\rangle_B - |\boldsymbol{r}\rangle_A|R\boldsymbol{r}\rangle_B + |R\boldsymbol{r}, \boldsymbol{r}\rangle_B - |R\boldsymbol{r}, \boldsymbol{r}\rangle_A]. \end{aligned} \tag{7}$$

We post-select on coincidences, allowing us to drop the latter two terms in equation (7), so

$$|\Psi_{\rm bs}\rangle = \mathcal{K}\sum_{\boldsymbol{r}} c(\boldsymbol{r})[|R\boldsymbol{r}\rangle_A|\boldsymbol{r}\rangle_B - |\boldsymbol{r}\rangle_A|R\boldsymbol{r}\rangle_B], \tag{8}$$

with $\mathcal{K}$ the normalisation constant.

A comparison of all the imaging scenarios will be easier if all R dependence is moved to photon B. In the supplementary material we demonstrate how the rotational dependence can be shifted from photon A to photon B, substituting R by R^{-1}, so equation (8) can be written as

$$|\Psi_{\rm bs}\rangle = \mathcal{K}\sum_{\boldsymbol{r}} c(\boldsymbol{r})|\boldsymbol{r}\rangle_A[|R^{-1}\boldsymbol{r}\rangle_B - |R\boldsymbol{r}\rangle_B]. \tag{9}$$

We therefore predict that ghost imaging with an HOM filter setup will produce a result consisting of a juxtaposition of the original object O rotated by an angle 2θ, and O rotated by -2θ.

3.2. BS without an HOM filter

To affect HOM filtering, it is experimentally necessary to make use of a BS and perfectly match the lengths of paths A and B. Photons A and B then have identical time stamps and are indistinguishable. All of this gives rise to the well-known 'HOM dip'.

However, we wish to study the effect of turning off the HOM filtering, but leaving the BS in place. This is achieved by slightly increasing the length of path B by way of the translation stage (the delay in figure 1) so that the difference in path length is larger than the coherence length of the SPDC detected photons. Photon B is ergo slightly delayed with respect to photon A and the photons are distinguishable. We indicate the presence of this time delay of photon B by means of a prime symbol, $|\boldsymbol{r}\rangle_B \rightarrow |\boldsymbol{r}'\rangle_B$. Effecting this change in photon B in equation (4) while applying the BS transformations in equation (6), and thereafter post-selecting on coincidences, gives

$$|\Psi'_{\rm bs}\rangle = \mathcal{K}\sum_{\boldsymbol{r}} c(\boldsymbol{r})[|R\boldsymbol{r}\rangle_A|\boldsymbol{r}'\rangle_B - |\boldsymbol{r}'\rangle_A|R\boldsymbol{r}\rangle_B]. \tag{10}$$

Be that as it may, since the object masking SLM_A is static and the time taken for each step of the measurement protocol carried out using SLM_B is orders of magnitude larger than the time taken for photon B to travel the extra distance of the mismatched path B, experimentally, the time delay of photon B cannot be observed. Therefore, results obtained for the mismatched path length case (i.e. with a non-zero θ and BS present, but no HOM filtering) appear identical to the HOM filtering case, so $|\Psi'_{\rm bs}\rangle \equiv |\Psi_{\rm bs}\rangle$.

3.3. Object reconstruction

Given either engineered state $|\Psi_{\rm nbs}\rangle$ or $|\Psi_{\rm bs}\rangle$, the detection section of the experiment is carried out by masking SLM_A with a binary object O, the information of which is contained in the function $O(\boldsymbol{r})$: $O(\boldsymbol{r}) = 0$ if the pixel at position $\boldsymbol{r}$ in SLM_A is black in the object, and 1 if pixel $\boldsymbol{r}$ is white. Here, black means the SPDC photons are blocked (or deviated from the optical axis to be more precise) and white means the reflected photons are properly detected. The operator describing this masking process is $|O\rangle_A = \mathcal{N}\sum_{\boldsymbol{r}} O(\boldsymbol{r})|\boldsymbol{r}\rangle_A$, with $\mathcal{N}$ the appropriate normalization. After masking SLM_A with O and absorbing $\mathcal{K}$ into $\mathcal{N}$, the state of photon B, in the absence of the BS, is

$$\langle O|\ \Psi_{\rm nbs}\rangle = \mathcal{N}^*\sum_{\boldsymbol{r}} c(\boldsymbol{r})O(R\boldsymbol{r})|\boldsymbol{r}\rangle_B. \tag{11}$$

In the case of HOM filtering, as well as the case of a non-zero θ-BS combination but mismatched path lengths, the state is

$$\langle O|\ \Psi_{\rm bs}\rangle = \mathcal{N}^*\sum_{\boldsymbol{r}} c(\boldsymbol{r})[O(R\boldsymbol{r}) - O(R^{-1}\boldsymbol{r})]\ |\boldsymbol{r}\rangle_B. \tag{12}$$

If we set the weighting coefficients c to unity, we can visualize the outcome more clearly

$$\langle O|\ \Psi_{\rm nbs}\rangle \propto \sum_{\boldsymbol{r}} O(R\boldsymbol{r})|\boldsymbol{r}\rangle_B, \tag{13}$$

$$\langle O|\ \Psi_{\rm bs}\rangle \propto \sum_{\boldsymbol{r}} [O(R\boldsymbol{r}) - O(R^{-1}\boldsymbol{r})]\ |\boldsymbol{r}\rangle_B, \tag{14}$$

where the operator $R = R(2\theta)$ is the rotation in the transverse plane. Both of these formulae match the earlier predictions, namely: a single image rotated relative to the object in the case of equation (13), and a juxtaposed 'double' image with opposite rotations in the case of equation (14). The intensity of pixel $|\boldsymbol{r}\rangle_B$ in the reconstructed object in each case is respectively

$$|\ \langle \boldsymbol{r}|_B\langle O|\ \Psi_{\rm nbs}\rangle|^2 \propto |O(R\boldsymbol{r})|^2, \tag{15}$$

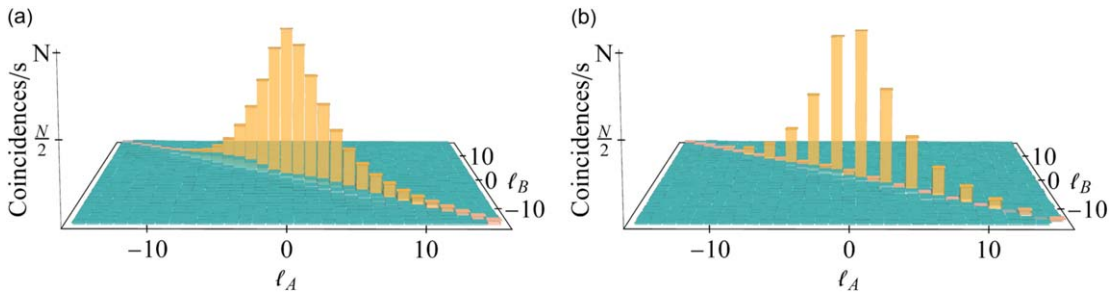

Figure 2. Experimental symmetry spatial filter by means of an HOM measurement within the OAM topological charge range $\ell_A = \ell_B = [-15,\ 15]$. (a) OAM spiral bandwidth of the SPDC photons when no HOM filtering is implemented, and (b) the analogous spiral bandwidth after introducing the HOM filter and setting the relative angle between the Dove prisms to $\theta = \frac{\pi}{4}$. The coincidence counts are normalized with respect to their respective maxima.

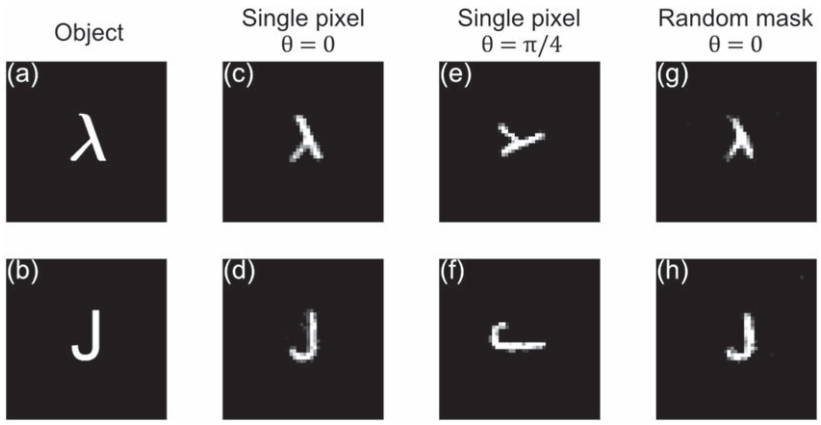

Figure 3. Ghost imaging results, with no BS ($|\Psi_{\rm nbs}\rangle$), using the SLM to encode the masks. (a), (b) The objects O encoded in path A, with white pixels indicating transmitted photons and the black pixels blocked photons. The reconstructed image of the corresponding object on the left, (c)–(f) using a single pixel 48 × 48 scan and the relative Dove prism angle in equation (2) set to (c), (d) $\theta = 0$ and (e), (f) $\theta = \frac{\pi}{4}$, or (g), (h) using a random mask scan with the same resolution and angle $\theta = 0$ as in (c), (d).

$$|\langle \boldsymbol{r}|_B \langle O|\ \Psi_{\rm bs}\rangle|^2 \propto |O(R\boldsymbol{r}) - O(R^{-1}\boldsymbol{r})|^2. \tag{16}$$

Equations (15) and (16) are key to understanding the object reconstructions shown in the following section.

4. Results and discussion

First we confirm the SPDC spiral bandwidth and the HOM filtering (the first two sections of the experiment in figure 1), with the results given in figure 2. Here, the OAM spiral bandwidth of the SPDC photons is experimentally measured within the range $\ell_A = \ell_B = [-15,\ 15]$, with the data in figure 2(a) taken without a BS, and that of figure 2(b) taken after introducing a BS and setting $\theta = \frac{\pi}{4}$, forming an HOM filter.

In what is to follow, we analyze the most important experimental results as predicted in the theory section. We first give the reconstructed object obtained in a standard ghost imaging setup, but instead use the SLM to dynamically encode the masks needed for each measurement. Next we show the effect of rotating one of the Dove prisms with respect to the other, and finally we implement the HOM filter before performing ghost imaging.

4.1. Rotated ghost imaging reconstruction

First, an experiment was run with the setup as depicted in figure 1, but without the HOM filter (the BS was removed). The SLM in path A was masked with a 960 × 960 resolution object O, as shown in figures 3(a), (b), while performing a digital raster scan using the SLM in path B (with a 48×48 resolution 'on pixel'). The results are shown in figures 3(c), (d) with a Dove prism angle of $\theta = 0$ and in figures 3(e), (f) when $\theta = \frac{\pi}{4}$. The ghost images were reconstructed using the set of coincidence counts $\{ c_i \}$ for every raster position in SLM_B as

$$\text{Image} = \frac{c_1}{n}P_1 + \frac{c_2}{n}P_2 + \cdots, \tag{17}$$

where c_i is the coincidence count recorded for raster position P_i, and n is a normalization constant (see supplementary material). The results confirm the accuracy of the digital scan approach. However, the resolution that can be used in such a single 'on pixel' reconstruction technique is limited by the strength of the signal arriving at the SLM. The integration time for each raster position increases as the pixel size decreases, in order to overcome the noise.

A different measurement scheme, a random mask scan [24] based on the compressed sensing concept [25], was also tested for the object reconstruction in order to overcome the noise in low signal cases without the need to decrease the resolution [26], as shown in the examples of figures 3(g), (h). As before, SLM_A is masked with a static 960×960 binary object O. However, instead of scanning over every pixel in SLM_B individually and recording the corresponding coincidence count, the random mask scheme involves first generating a set of N random binary masks, with 50% of the pixels white and 50% of the pixels black, randomly so, for each mask. Then, SLM_B is encoded with one of these random binary masks and the corresponding coincidence counts recorded. This process is repeated for every random mask. Finally, with the set of random binary masks $\{ M_i \}$ and their corresponding coincidence counts $\{ c_i \}$, for a large enough N, the object is reconstructed by again taking a convex combination of images, with the images in this scheme being the weighted random masks themselves, i.e.

$$\text{Image} \approx \frac{(c_1 - \bar{\boldsymbol{c}})}{n}M_1 + \frac{(c_2 - \bar{\boldsymbol{c}})}{n}M_2 + \cdots, \tag{18}$$

where c_i is the coincidence count recorded for each random mask M_i, n is a normalization constant, and $\bar{\boldsymbol{c}}$ is the average of all coincidence counts measured [26]. This is done since the 'on' pixel would ordinarily correspond to a value of 1 and the 'off' pixel to -1, giving an average outcome of 0. But in our case, the 'off' pixel corresponds to 0, thus the non-zero average values must be subtracted to remove the noise. An animated example of the random mask reconstruction of figure 3(g) can be observed in the attached animation file (Lambda reconstruction), where the object is given in the leftmost, the real random mask used for each scan (iteration) is given in the middle, and the reconstructed image appears in the rightmost. The reconstructed image becomes clearer as the number of iterations, shown at the top, increase.

It is worth mentioning that this scheme can be generalised to cases with arbitrary proportions of black: white pixels. As we decrease the proportion of white pixels, we decrease the average of the measured coincidences which needs to be subtracted, i.e. the measurements are less noisy when not performing the average subtraction, with the extreme case being only 1 pixel as in equation (17). However, the maximum attainable resolution decreases, for a given signal arriving at the SLM, when decreasing the proportion of white pixels.

To test this measurement technique in a ghost imaging setup, the experiment was run with the objects given in figures 4(a)–(d), using $N = 4000$ different random masks, recording the coincidences with an integration time of 1 second per mask, and setting the relative Dove prism angle to $\theta = \frac{\pi}{4}$ for the results in figures 4(e)–(h), and $\theta = -\frac{\pi}{8}$ for those in figures 4(m)–(p).

From these results, the reconstructed image is rotated by an angle of 2θ with respect to the original object, as predicted in equation (15). This confirms the effect of Dove prisms on ghost imaging and lends credence to the idea of performing such calculations in the chosen position basis.

4.2. Double ghost images

Next, to implement an HOM filter and investigate its effect on the reconstructed image, the relative Dove prism angle was set to a non-zero value and a BS inserted into the setup, which selects the state $|\Psi_{\text{bs}}\rangle$. As per equation (16), the intensity of pixel $\boldsymbol{r}$ in the reconstructed image is a combination of the intensity of pixel $\boldsymbol{r}$ in O, rotated by both $R(2\theta)$, and by $R^{-1}(2\theta) = R(-2\theta)$. As stated, the reconstructed image will hence be a juxtaposition of O rotated by 2θ and O rotated by -2θ. This is confirmed experimentally in figures 4(i)–(l) for a relative Dove prism angle of $\theta = \frac{\pi}{4}$, and in figures 4(q)–(t) for $\theta = -\frac{\pi}{8}$.

The experimental results in each row are for the objects given in the first column. Note that the results in the last row of figure 4 are identical, with or without the BS and $\theta = \frac{\pi}{4}$, and match the intensity profile of the object, save for the rotation. In other words, we do not see the 'double' image in the reconstructed images. This is a result of the original object being invariant under a rotation by π. This image invariance under rotations could play a role in future applications where the study of the innate geometric symmetry of an object is important, or it may find application in the field of quantum communication, wherein one could ascertain the centre of an SPDC beam source and align a system accordingly by using the counter-rotated reconstructed object.

Note that the experimental results slightly differ from their simulations shown in the insets, due to the difference in reflection/transmission ratios of the BS. We expect this to be the reason of the anti-clockwise-rotated portion of the reconstructed image to be dimmer compared with the clockwise-rotated portion; each

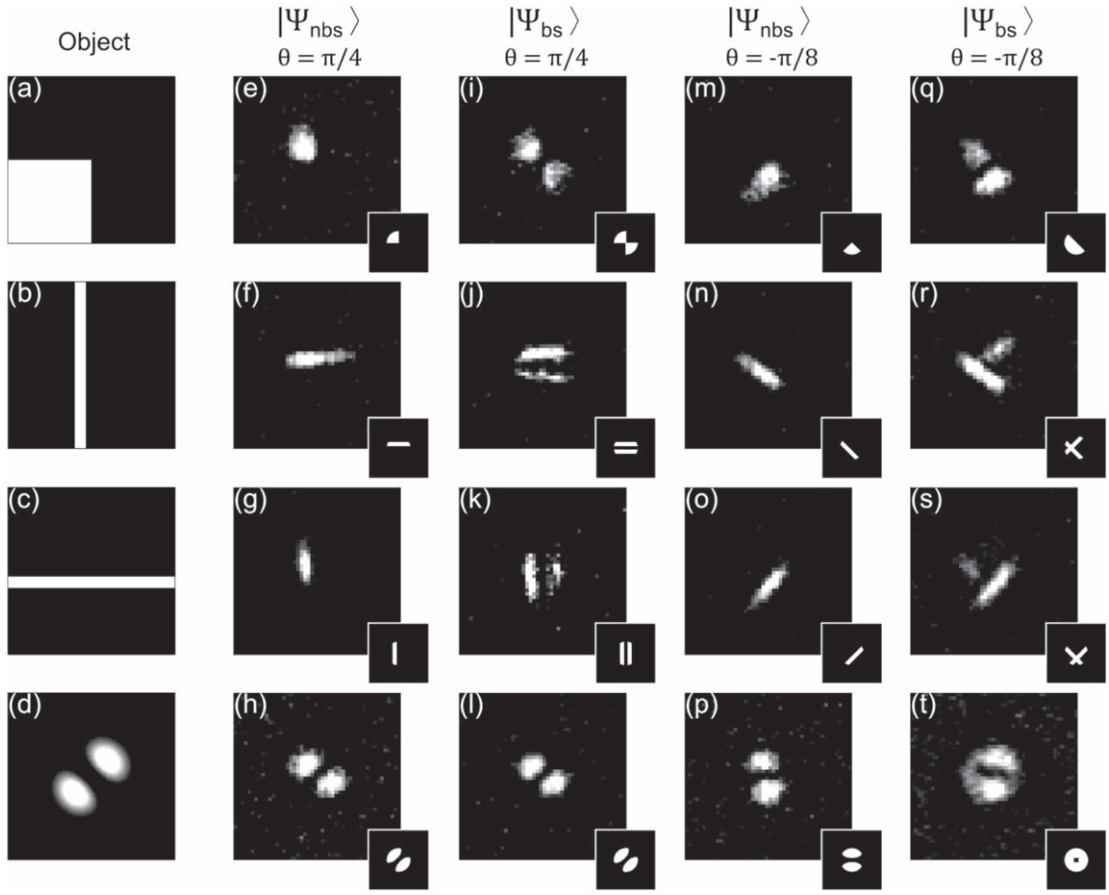

Figure 4. Ghost imaging with and without HOM filtering, using the random mask scan sequence with 48 × 48 resolution. (a)–(d) The objects O encoded in SLM_A. (e)–(h), (m)–(p) The reconstructed image results considering the objects on the leftmost without a BS and (e)–(h) $\theta = \frac{\pi}{4}$ or (m)–(p) $\theta = -\frac{\pi}{8}$. (i)–(l), (q)–(t) The reconstructed image of the leftmost objects including a coherent superposition at the BS and (i)–(l) $\theta = \frac{\pi}{4}$ or (q)–(t) $\theta = -\frac{\pi}{8}$. Insets show the simulated results taking into account a perfect aligned projections and the overlap with the 5 mm diameter SPDC beam.

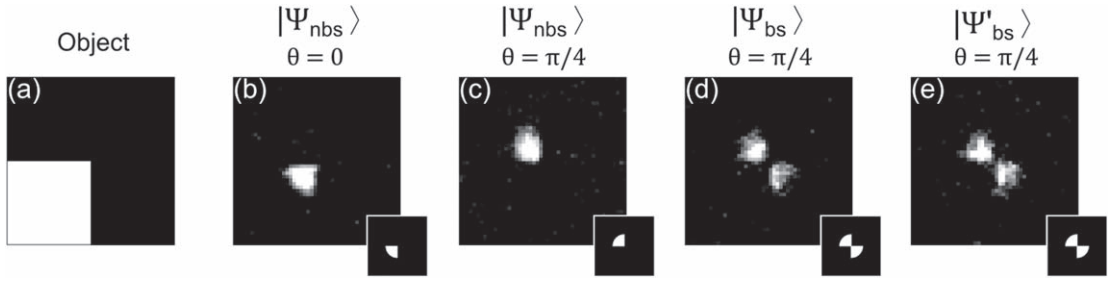

Figure 5. Ghost imaging result summary. (a) Object; (b) no Dove prisms nor BS; (c) $\theta = \frac{\pi}{4}$ but no BS; (d) $\theta = \frac{\pi}{4}$ and HOM filter (BS present and path lengths matched), and (e) $\theta = \frac{\pi}{4}$, BS present, but with the length of path B slightly increased in order to obtain measurements without the symmetry filtering.

half of the SPDC state, one in arm A and the other in arm B, traverses different ports of the BS. On the other hand, we deliberately displaced the object from the SPDC beam center of coordinates adding extra space between the reconstructed images, to properly identify the double rotation effect.

Finally, figure 5 gives a summary of all possible scenarios considered with the setup in figure 1. In particular, the image in figure 5(e) was recorded after the length of path B was increased by 100 μm in order to remove the HOM effect but keeping the BS in. That is to say, figure 5(e) shows the results for the $|\Psi'_{bs}\rangle$ state. It was anticipated that $|\Psi_{bs}\rangle \equiv |\Psi'_{bs}\rangle$, which is confirmed experimentally given the fact that figures 5(d) and (e) are qualitatively identical.

This image doubling can be understood as the BS 'splitting' the image in two, and then being recombined after changing the path conditions. When measured in coincidence, a rotated photon A is either transmitted by the BS and interacts with the object, in which case the unrotated photon B (whose phase is -2θ with respect to photon A) is measured by the detection scheme, or the unrotated photon B is reflected by the BS and interacts with the object, with the rotated photon A (with a 2θ phase relative to photon B) being measured.

Moreover, such 'splitting' of the object into two rotated images is not restricted to any specific optical plane. This was tested by moving the BS to the Fourier plane of the crystal (and the SLM), with the results obtained in such a case identical to those reported here for the image plane.

5. Conclusions

We have used an HOM filter to engineer particular quantum states and used them in ghost imaging experiments. The results are in agreement with the theory and confirm the image rotation and image 'doubling' as a consequence of the state preparation. Although such filtering is often understood in terms of the OAM basis, we translate it here to the position basis by virtue of the invariance of a quantum state's intrinsic symmetry under basis changes. In addition to an intriguing ghost imaging setup, we also employ all-digital control over the imaging arm for fast and convenient image reconstruction. Our work highlights important aspects of this form of ghost imaging and paves the way for further investigations and applications that employ imaging with specially engineered states.

Acknowledgments

The authors would like to thank FS Roux, M Agnew, MJ Padgett and M Hendrych for valuable discussions. NB acknowledges financial support from the South African CSIR DST-IBS programme and AV from the Claude Leon Foundation.

ORCID iDs

Adam Vallés https://orcid.org/0000-0002-5200-4914
Andrew Forbes https://orcid.org/0000-0003-2552-5586

References

[1] Pittman T, Shih Y, Strekalov D and Sergienko A 1995 *Phys. Rev.* A **52** R3429
[2] Walborn S P, Monken C, Pádua S and Ribeiro P S 2010 *Phys. Rep.* **495** 87–139
[3] Bennink R S, Bentley S J and Boyd R W 2002 *Phys. Rev. Lett.* **89** 113601
[4] Bennink R S, Bentley S J, Boyd R W and Howell J C 2004 *Phys. Rev. Lett.* **92** 033601
[5] Valencia A, Scarcelli G, D'Angelo M and Shih Y 2005 *Phys. Rev. Lett.* **94** 063601
[6] Gatti A, Brambilla E, Bache M and Lugiato L A 2004 *Phys. Rev. Lett.* **93** 093602
[7] Cai Y and Zhu S Y 2005 *Phys. Rev.* E **71** 056607
[8] Erkmen B I and Shapiro J H 2010 *Adv. Opt. Photonics* **2** 405–50
[9] Shapiro J H 2008 *Phys. Rev.* A **78** 061802
[10] Katz O, Bromberg Y and Silberberg Y 2009 *Appl. Phys. Lett.* **95** 131110
[11] Jack B, Leach J, Romero J, Franke-Arnold S, Ritsch-Marte M, Barnett S and Padgett M 2009 *Phys. Rev. Lett.* **103** 083602
[12] Ryczkowski P, Barbier M, Friberg A T, Dudley J M and Genty G 2016 *Nat. Photon.* **10** 167
[13] Howell J C, Bennink R S, Bentley S J and Boyd R 2004 *Phys. Rev. Lett.* **92** 210403
[14] Chan K W C, O'Sullivan M N and Boyd R W 2009 *Phys. Rev.* A **79** 033808
[15] Sun B, Edgar M P, Bowman R, Vittert L E, Welsh S, Bowman A and Padgett M 2013 *Science* **340** 844–7
[16] Cheng J 2009 *Opt. Express* **17** 7916–21
[17] Shapiro J H and Boyd R W 2012 *Quantum Inf. Process.* **11** 949–93
[18] Moreau P A, Toninelli E, Gregory T and Padgett M J 2019 *Nat. Rev. Phys.* **1** 367–80
[19] Bornman N, Agnew M, Zhu F, Vallés A, Forbes A and Leach J 2018 arXiv:1809.0258
[20] Hong C K, Ou Z Y and Mandel L 1987 *Phys. Rev. Lett.* **59** 2044
[21] Allen L, Padgett M and Babiker M 1999 Iv the orbital angular momentum of light *Progress in Optics* vol 39 (Amsterdam: Elsevier) pp 291–372
[22] Zhang Y, Roux F S, Konrad T, Agnew M, Leach J and Forbes A 2016 *Sci. Adv.* **2** e1501165
[23] Zhang Y, Prabhakar S, Rosales-Guzmán C, Roux F S, Karimi E and Forbes A 2016 *Phys. Rev.* A **94** 033855
[24] Chan W L, Charan K, Takhar D, Kelly K F, Baraniuk R G and Mittleman D M 2008 *Appl. Phys. Lett.* **93** 121105
[25] Donoho D L 2006 *IEEE Trans. Inf. Theory* **52** 1289–306
[26] Sun M J, Edgar M P, Phillips D B, Gibson G M and Padgett M J 2016 *Opt. Express* **24** 10476–85